Interpreting granulite facies events through rare earth element partitioning arrays

Interpreting granulite facies events through rare earth element partitioning arrays

R.J.M. TAYLOR[1], C. CLARK[1], S.L. HARLEY[2], A.R.C. KYLANDER-CLARK[3], B.R. HACKER[3], P.D. KINNY[1]*

1. Department of Applied Geology, Western Australian School of Mines, Curtin University, Bentley, Perth WA, Australia

2. School of Geosciences, Kings Buildings, West Mains Road, Edinburgh, UK

3. Department of Earth Science, University of California, Santa Barbara, CA 93106, USA

Corresponding author email id: richard.taylor@curtin.edu.au

Abstract

The use of rare earth element (REE) partition coefficients is an increasingly common tool in metamorphic studies, linking the growth or modification of accessory mineral geochronometers to the bulk silicate mineral assemblage. The most commonly used mineral pair for the study of high-grade metamorphic rocks is zircon and garnet. The link from U–Pb ages provided by zircon to the *P-T* information recorded by garnet can be interpreted in relation to experimental data. The simplistic approach of taking the average REE abundances for zircon and garnet and comparing them directly to experimentally derived partition coefficients is imperfect, in that it cannot represent the complexity of a natural rock system. This study describes a method that uses all the zircon analyses from a sample, and compares them to different garnet compositions in the same rock. Using the most important REE values, it is possible to define zircon–garnet equilibrium using an array rather than an average. The array plot describes partitioning between zircon and garnet using D_{Yb} and D_{Yb}/D_{Gd} as the defining features of the relationship. This approach provides far more sensitivity to mineral reactions and diffusional processes, enabling a more detailed interpretation of metamorphic history of the sample.

KEYWORDS

Rare earth elements; petrochronology; zircon; garnet; orthopyroxene

This article has been accepted for publication and undergone full peer review but has not been through the copyediting, typesetting, pagination and proofreading process, which may lead to differences between this version and the Version of Record. Please cite this article as doi: 10.1111/jmg.12254

1. | INTRODUCTION

For 15 years, rare earth element (REE) partitioning between zircon and garnet has facilitated the coupling of U–Pb ages to metamorphism (Rubatto, 2002), particularly in the granulite facies (Buick et al., 2006; Harley et al., 2001; Hermann and Rubatto, 2003; Hokada and Harley, 2004; Kelly and Harley, 2005; Taylor et al., 2015a; Whitehouse and Platt, 2003). The combination of *in situ* analysis and rapid data acquisition, particularly through combined techniques such as laser ablation split stream (LASS) (Kylander-Clark et al., 2013), means that complex terranes can be interrogated with increasing detail. However the detail provided by large datasets must be tempered with an understanding of the processes involved—for example the relative mobility of the REE, Ti, U and Pb (Cherniak et al., 1997; Cherniak and Watson, 2001, 2003, 2007)—and an appreciation that these data represent zircon which has withstood intense *P–T* conditions to varying degrees (Clark et al., 2009; Timms et al., 2011). The acknowledgement that metamorphic zircon crystallizes or recrystallizes in response to a variety of mineral reactions, as well as melt and fluid related processes is critical in the interpretation of a metamorphic zircon age (Harley et al., 2007; Kelsey et al., 2008; Roberts and Finger, 1997; Rubatto et al., 2001; Taylor et al., 2014).

Care must also be taken in studies of granulite facies rocks to identify open system conditions and the response of accessory phases to anatexis, for example the prolonged presence of melt or multiple episodes of partial melting that result in non-equilibrium, or very localised equilibrium, among the phases of interest (Ashwal et al., 1999; Clark et al., 2015; Gordon et al., 2016; Harley and Nandakumar, 2014; Johnson et al., 2015; Korhonen et al., 2013, 2014; Raith et al., 2016; Yakymchuk et al., 2015). Other scenarios that may create inter-grain heterogeneity must also be taken into account when using trace elements to interpret geochronological data. This may include, but is not limited to, the nature of each grain's internal zoning (Corfu et al., 2003; Taylor et al., 2016), post-growth diffusion processes and grain interface diffusion rates (e.g. Ague and Baxter, 2007; Dempster et al., 2017; Watson and Baxter, 2007), and reactions involving other trace element rich reservoirs (e.g. Hermann and Rubatto, 2003; Hermann and Rubatto, 2009; Pyle and Spear, 2003; Watt and Harley, 1993), all of which may affect major and accessory mineral compositions.

Visualisation of REE partition coefficients (D_{REE}) becomes more difficult with large datasets particularly when dealing with variably recrystallized zircon or multiple generations of garnet. Traditional methods of visualising REE partitioning data (or REE data in general), such as the chondrite normalised REE plot, become unwieldy with larger datasets, often masking simple trends. This leads to simplifications—such as deriving an average REE value for a suite of zircon analyses in order to distinguish metamorphic/recrystallized populations (e.g. Estrada-Carmona et al., 2016; Fornelli et al., 2014; Harley and Kelly, 2007; Hokada and Harley, 2004; Raith et al., 2016; Štípská et al., 2016; Taylor et al., 2015a). This simple approach is often inadequate at describing the complexity in empirical metamorphic datasets.

In this study we propose a new approach, utilising data from all zircon analysed, to identify the key partitioning parameters relevant to the problem at hand. In the case of REE partitioning between zircon and garnet ($D_{REE(zircon–garnet)}$), the behaviour of middle to heavy rare earth elements (M–HREE)—as recorded in the absolute values of

D_{HREE}, and the slope from the MREE to HREE—is of prime importance. We describe a simple method of visualising important partitioning parameters that highlight temperature trends in experimental datasets (Rubatto and Hermann, 2007; Taylor et al., 2015b). These trends can be used as indicators of zircon growth or recrystallization in the presence of stable garnet or orthopyroxene. Investigation of D_{REE}*(zircon–garnet)* values in both long-lived high-grade terranes (e.g. Southern Granulite Terrane, S. India), and complex polymetamorphic terranes (e.g. Enderby Land, E. Antarctica) provides insight into how partitioning information can be carefully interrogated by comparing to experimental data, or by looking at systematic or erratic variations from experimental data, even when dealing with issues such as variably recrystallized zircon, elemental diffusion, and melt migration. These case studies investigate metamorphic zircon both neocrystallized and recrystallized in the high-*T* granulite facies, particularly at ultrahigh temperature (UHT) conditions, however the same approach could be applied to use at lower temperatures or in high–*P* terranes with the aid of additional experimental constraints or modelling.

2. | VISUALISING EXPERIMENTAL REE PARTITIONING DATA

Two experimental datasets aid the interpretation of zircon–garnet relationships in metamorphic rocks (Rubatto and Hermann, 2007; Taylor et al., 2015b). Both datasets show some degree of temperature control on the D_{REE} values between these two key minerals. The experiments of Rubatto and Hermann (2007) at 20 kbar show an order-of-magnitude variation of D_{HREE} values over the temperature range 800–1000°C. In these experiments there is also a factor of 2–3 variation in MgO and CaO concentrations in garnet. Whilst chemical variation is inherent in natural systems it leaves ambiguity as to the relative roles that temperature and bulk/garnet chemistry have on D_{HREE}*(zircon–garnet)* values. The later experiments of Taylor et al. (2015b) at 7 kbar and 900–1000°C show a more limited D_{HREE} variation, again with higher temperatures favouring HREE incorporation into garnet. These experiments were on Ca-free, almandine-pyrope garnet with minimal chemical variation. This may suggest that chemistry exerts a greater control on the partitioning values than temperature, however the (Taylor et al., 2015b) experiments were over a narrower temperature range (900–1000°C) specific to UHT metamorphism, potentially limiting extrapolation to lower temperature. The different pressure of the two experimental datasets, tailored to the particular geological conditions simulated by these groups (HP-HT and UHT-LP respectively), may also have resulted in the differences seen between the two datasets.

Figure 1 shows the experimental D_{REE}*(zircon–garnet)* data from Rubatto and Hermann (2007) and Taylor et al. (2015b) on a traditional REE partitioning plot, in which zircon REE values are normalised to that in garnet (values for plotting 7 kbar data can be found in Table 1). D_{REE} data are most commonly visualised using this traditional plot with D_{REE} values shown sequentially from La to Lu, showing partition coefficients for all REE. The typical way that experimental D_{REE}*(zircon–garnet)* datasets are used to evaluate empirical data, is to overlay them on natural datasets and gauge their similarity. This approach is simple but can be sufficient to distinguish metamorphic zircon, particularly in unzoned, neocrystallized populations. However this method may become inadequate in terranes that have undergone polymetamorphism, may have more than one garnet generation, or have metamorphic zircon rims formed by recrystallization (rather than new growth), and varying degrees of chemical re-equilibration. In this situation, as samples become more complex, it becomes necessary

to take far more care observing individual grains within their textural context in thin section. Even with such petrographic observation it may be difficult to determine individual zircon generations, particularly as an average REE pattern is often used for each zircon population (e.g. Harley and Kelly, 2007).

In order to handle larger empirical datasets in a practical manner it is essential to distil the standard REE diagram into a plot of two key parameters which together can represent the shape and REE abundance of the original partitioning plot. Both zircon and garnet contain abundant M–HREE and these elements are the most sensitive to changing environmental conditions, making them a key for identifying metamorphic zircon. Therefore in order to describe the $D_{REE(zircon–garnet)}$ relationship, we plot the slope from the M–HREE (D_{Yb}/D_{Gd}), against D values for a HREE (D_{Yb}) (Figure 2a). The elements Gd and Yb are chosen as they have even atomic numbers, hence are more abundant and therefore provide more robust data. As the parameters are ratios of the REE, we plot the log values to preserve the symmetry of variations above and below unity, resulting in a plot of $\log(D_{Yb}/D_{Gd})$ versus $\log(D_{Yb})$. These two parameters have been chosen deliberately as the relationship between them may covary, resulting in potential $D_{REE(zircon–garnet)}$ relationships that are clearly distinguishable on the array plot (Figure 2b).

Figure 3 shows the experimental data (Rubatto and Hermann, 2007; Taylor et al., 2015b) in this new array plot. The experimental data show covariance between the parameters, providing a simple visual framework against which empirical data can be interpreted. The plotted parameters show a trend that appears to be temperature dependent, with both datasets showing the highest temperature experiments at the lowest values. D_{Gd} and D_{Yb} values from Taylor et al. (2015b) are the lattice strain modelled values derived from that study, considered to be the most robust version of the 7 kbar dataset, to which empirical data can be compared. It must be noted that even though the experimental data can be used as a direct reference frame to which empirical data can be compared, there are many caveats as to the nature of experimental chemical equilibrium, such as the experiment timeframe, and the mixed analysis required to gain zircon REE patterns. The experimental studies (Rubatto and Hermann, 2007; Taylor et al., 2015b) discuss at some length the methods employed to give confidence to the fact that they represent a close proximity to REE equilibrium, however a cautious approach must always to be taken to avoid over-interpretation of the similarities between experiments, that have significant uncertainty on the analytical data, and empirical samples.

3. | VISUALISING NATURAL EXAMPLES

In order to obtain the most information from any empirical dataset it is preferable to use every zircon analysis, and to evaluate the U–Pb isotopic data in relation to the trace element data obtained from the same grain/zone (e.g. SIMS U–Pb followed by LA-ICPMS; SIMS-U–Pb followed by SIMS-TE), or even better from the same sample volume, with isotope and trace element data obtained simultaneously using Laser Ablation Split Stream (LASS) (Kylander-Clark et al., 2013). The fact that the experimental data form a trend when plotted using these parameters provides a method for evaluating empirical D_{REE} data. The first test for assessing the experimental trend is a comparison with some well-constrained geological examples plotted to assess whether natural zircon–garnet relationships form arrays like the experimental data or simpler clusters. During the T–t evolution of a rock, zircon growth is not instantaneous. Even in a simple case where

growth is due to a single process, e.g. Zr saturation during melt crystallization, zircon growth takes time and may involve scenarios such as armouring of grains within other phases. Hence different grains may reflect growth at different temperature, and compositional environments, creating an array even for a single age population.

The method employed here enables every analysis of 'mineral 1' to be plotted against a single 'mineral 2' composition. In general there is more complexity in zircon REE compositions than garnet. Additionally, as a major silicate mineral, garnet populations can be more directly ascribed to a geological process. It is therefore beneficial to use each analysis for zircon, and compare them to individual garnet compositions. There is however no limit to the detail at which garnet variation can be probed, with clear compositional populations an average may suffice, or end member compositions could be used. In the majority of studies investigated here every zircon analysis is plotted against an average garnet composition. For all the following examples the empirical data are compared to the experimental data of Taylor et al. (2015b) seen in Figure 3, which are the most relevant to the high-*T*, low-*P* conditions studied.

3.1 | Examples from the Southern Granulite Terrane, S. India

3.1.1 | Post-peak melt crystallization

The crystallization of anatectic melt in a garnet-bearing rock provides an ideal setting for the crystallization of zircon in equilibrium with the rims of peritectic garnet (e.g. Taylor et al., 2015a). Whilst it makes sense that the garnet rims are in textural equilibrium with final melt crystallization, the variation in REE composition may be minor from core to rim, and so this forms a good test case to assess whether an array plot provides a better test of equilibrium partitioning than a standard REE diagram. Figure 4 shows data from an ultrahigh-temperature (UHT) garnet–orthopyroxene metapelite from the Achankovil Zone, southern India (Taylor et al., 2015a), interpreted to have formed on a clockwise *P*–*T* path with peak conditions of ~7 kbar and 950°C. The normalised REE concentrations for zircon detrital cores and metamorphic rims, and for garnet cores and rims (Figure 4a,b) show a relatively simple scenario.

Zircon growth at *c*. 513 Ma was interpreted in the study to be due to post peak-*T* melt crystallization (Taylor et al., 2015a). Plotting the D_{REE} data on traditional REE plots (Figure 4c – zircon/garnet cores; Figure 4d – zircon/garnet rims) produces typical patterns, with sloping D_{HREE} for the detrital zircon cores, and flat D_{M-HREE} patterns with values ~1 for the for metamorphic zircon rims. This supports the assertion that the zircon rims are in equilibrium with metamorphic garnet based on the experimental data of Taylor et al. (2015b). However the two plots are similar, in both cases overlapping the experimental data of Taylor et al. (2015b) demonstrating chemical equilibrium for metamorphic zircon with either garnet cores or rims. The differences become more apparent when displayed on the array plot (Figure 4e – zircon/garnet cores; Figure 4f – zircon/garnet rims). The detrital zircon data form a cloud of points with little to no systematic variation, whereas the metamorphic zircon data form a distinct linear trend, parallel to the experimental data from (Taylor et al., 2015b). Whilst there is no direct need to observe the detrital data in this sample, it serves as a good example that the linear arrays are not a ubiquitous result of the method used. When plotted against the garnet cores (Figure 4e) the metamorphic zircon is offset from the experimental array, however when plotted against the garnet rims (Figure 4f) the metamorphic zircon data

are a very close match. This example highlights the efficacy of the array plot to evaluating equilibrium zircon–garnet partitioning even in situations where variations in garnet composition are subtle.

3.1.2 | Multiple garnet generations

The array plot can also aid in the interpretation of multiple garnet generations. A garnet–cordierite gneiss, also from the Achankovil Zone of southern India (Taylor et al., 2015a), contains a single, *c*. 519 Ma zircon generation with a large spread in HREE (Figure 5a), and multiple garnet compositions. This sample is interpreted to have formed during the same clockwise *P–T* path with peak conditions of ~7 kbar and 950°C. Large, prograde garnet 1 has a depleted HREE composition, its modified rim has comparatively elevated HREE, and a smaller, second-generation garnet 2 displays the highest HREE (Figure 5b). Despite the large spread in zircon HREE, D_{REE} data still form a single partitioning array (Figure 5c,d). The garnet 1 core does not reflect equilibrium partitioning on either a conventional or array-style REE plot (not shown), however both the garnet 1 rims and garnet 2 compositions overlap the experimental data with the garnet 2 composition the sitting more centrally on the experimental data (Figure 5c,d).

3.1.3 | Non-equilibrium zircon growth

Under certain circumstances the metamorphic zircon that crystallizes may not be in equilibrium with the garnet in the same rock. A final example from Taylor et al. (2015a) is a garnet-bearing granite sheet that cross-cuts the metamorphic fabric of the previously described garnet–cordierite gneiss (peak conditions ~7 kbar and 950°C). As with the previous samples from this locality there are some inherited, Mesoproterozoic zircon and discordant/semi-concordant data extending towards a younger age. Inherited zircon and later metamorphic zircon display very similar M–HREE contents (Figure 6a), however the older/inherited grains typically have a smaller Eu anomaly and remain steeper through the HREE.

A coherent zircon age population of *c*. 525 Ma has a consistent REE pattern (Figure 6a), and garnet is also relatively homogenous (Figure 6b). Analyses in Figure 6 have been separated into those which show a more inherited/pre-garnet trace element signature (high Eu/Eu*; steeper HREE slope) and those which suggest growth/recrystallization in the presence of the low Eu/Eu* garnet-bearing rock (low Eu/Eu*; flatter HREE) (e.g. Kotková and Harley, 2010). Based on a traditional REE plot the average D_{HREE}*(zircon–garnet)* values are very close to the experimental data (Figure 6c) for both groups, and had therefore been interpreted as being close to chemical equilibrium (Taylor et al., 2015a). However the array plot shows a different story (Figure 6d); a weakly defined array that shows considerable scatter and a deviation from the experimental array in which any $D_{Yb}/D_{M–HREE}$ ratio is greater than the experimental trend. There is also a large amount of cross over between the high Eu and low Eu grains highlighting that slow diffusion during recrystallization of pre-existing zircon may not produce, chemically distinct populations.

3.1.4 | Local-scale equilibrium signatures

Metapelitic rocks in long-lived granulite facies terranes have the potential to grow and modify zircon and garnet throughout their metamorphic evolution due to a number of processes occurring during the local transfer or stagnation of small volumes of anatectic melt (e.g. Harley and Nandakumar, 2014). The resultant spread of zircon U–Pb ages has the potential to be interpreted as reflecting a single, long-lived event or partial resetting between separate high-*T* events. The Trivandrum Block of the Southern Granulite Terrane contains garnet–sillimanite-cordierite gneisses that were particularly fertile compositions for the growth/modification of zircon at high-*T* (6–8 kbar, 880–900°C; (e.g. Braun and Bröcker, 2004; Nandakumar and Harley, 2000)) during the Pan-African assembly of Gondwana *c*. 600–500 Ma (e.g. Blereau et al., 2016; Collins et al., 2014; Fonarev et al., 2000; Harley and Nandakumar, 2014, 2016; Santosh et al., 2006a,b; Tadokoro et al., 2008; Taylor et al., 2014). Figure 7a shows a zircon U–Pb concordia spread for a typical Trivandrum Block garnet–sillimanite-cordierite gneiss (from Taylor et al., 2016; Figure 5a) from the Kullapara quarry of Harley and Nandakumar (2014). All data for the Kullapara sample (I11-002) are in Table SA.

The spread of apparent metamorphic ages for the metapelite ranges from 588 ± 22 Ma to 494 ± 14 Ma (uncertainties at 2σ, Figure 7a). The metapelite zircon trace element compositions—such as REE (Figure 7b)—show no consistent patterns with U–Pb age and cover more than two orders of magnitude. Garnet compositions are also highly variable covering more than an order of magnitude within single thin section (Figure 7c). As with the previous example there is a distinct variation in Eu_N values in zircon, though with no age correlation. It is possible that zircon with large Eu anomalies represents neocrystallization in equilibrium with garnet, that also shows strong Eu anomalies. The zircon with smaller Eu anomalies may reflect recrystallized zircon with a pre-garnet Eu signature, due to the slower diffusion of MREE in zircon relative to Pb and HREE (Cherniak et al., 1997; Cherniak and Watson, 2001, 2003). The garnet REE broadly show three compositions: relatively speaking a low HREE group, a mid HREE group and a single HREE analysis representing the highest value for garnet in the sample. It is impossible to select a single D_{REE}*(zircon–garnet)* value without either arbitrarily choosing which values are "best" or taking an average of a very large range. To try and incorporate all the possibilities on a traditional REE plot would be unwieldy.

The array plot demonstrates that despite the large variation in zircon REE compositions, they all fall along a single array when plotted against any garnet composition. Using the alternative garnet compositions (low, mid, and high HREE) simply moves the array in relation to, but always overlapping, the experimental data (Figure 7d), even though Eu anomalies suggest there may be both neocrystallized and recrystallized grains. Despite the fact that here we have formed groups for the garnet analyses, the natural implication is that any single garnet analysis will form DREE values that fall on the experimental array. This implies that despite the spread of mineral trace element compositions, and lack of trends with age, all zircon compositions may have been in chemical equilibrium with at least some of the garnet in the sample, i.e. have shared independent evolutions with small, garnet-bearing volumes of the rock. As such this relationship on the array plot is likely to be the result of local–scale equilibrium, in which the complexity of small scale processes resulted in variable trace element compositions, but maintained chemical equilibrium between minerals over small distances.

3.2 | Examples from Enderby Land, E. Antarctica

The UHT rocks of Enderby Land in eastern Antarctica provide an opportunity to apply the array plot to rocks that have undergone multiple high temperature metamorphic events. The extreme conditions (7-11 kbar and >1000°C) endured during *c.* 2.8 Ga and *c.* 2.5 Ga granulite facies events resulted in modification of pre-existing zircon in rock with multiple generations of garnet, and in orthopyroxene-bearing assemblages (e.g. Black et al., 1986; Harley and Black, 1987, 1997; Harley, 1985; Hokada and Harley, 2004; Hokada et al., 2004; Kelly and Harley, 2005; Kusiak et al., 2013a,b). The samples from Enderby Land contain a high proportion of recrystallized zircon domains, compared to predominantly neocrystallized zircon overgrowths in the S. India examples. This difference is very important, a neocrystallized grain might be assumed to lock in an isotopic and elemental composition representing its time of formation. Whereas a recrystallized grain will inherently have less well-defined composition due to variable diffusion rates of U, Pb, REE, Ti etc and the necessity to either incorporate or shed these elements via diffusional and grain surface processes in an attempt to equilibrate with its environment. For this reason the Enderby Land samples were analysed using the LASS system at the University of California, Santa Barbara, collecting U–Pb, REE and Ti simultaneously (Kylander-Clark et al., 2013). Whilst LASS is not the only method that can be employed, the combination of a large analytical dataset with this simultaneous data collection is a powerful tool when dealing with recrystallized grains, as trends in the data may be more apparent, and anomalies more easily distinguished. Data from two samples from Crosby Nunatak in the Tula Mountains of Enderby Land are presented here to assess the benefits of using the array plot to assess trace element data. Both samples are quartz-bearing and contain abundant rutile, both exsolving from quartz and as large euhedral to subhedral grains up to 300μm, making it ideal for 4+ cation thermometry studies (Taylor et al., 2016). Trace element and U–Pb data tables for the Crosby samples are in Table S2.

3.2.1 | Crosby Nunatak – multiple partitioning arrays

Sample 171279/3 from Crosby nunatak is a garnet-bearing gneiss. A combination of U–Pb and trace element data from LASS analysis shows two distinct groups of zircon (Figure 8a). Zircon with steep chondrite normalised HREE patterns (Yb_N/Gd_N 10–22) range in age from 2849 ±34 Ma to 2509 ±36 Ma. Zircon with flat HREE patterns (Yb_N/Gd_N 1–5) form a distinct age population with a weighted mean $^{207}Pb/^{206}Pb$ age of 2451 ±15 Ma (95% conf.; MSWD = 1.2). The majority of the garnet in the sample has consistent, flat M–HREE patterns with Yb_N ~300–800 times chondrite; whereas a second generation of garnet associated with fine-grained leucosomes shows negatively sloping M–HREE patterns and Yb_N values down to ~40.

The array plot reveals that the main generation of flat HREE garnet is closest to being equilibrated with the *c.* 2451 Ma zircon, with an array close to the experimental data (Figure 8b). It is acknowledged the array is not a direct fit to the experimental data in this example, but the array clearly shows a zircon-garnet relationship. However, the most striking aspect of this plot is that the older, steep HREE zircon form a negatively sloping array in a perpendicular orientation to that expected from zircon–garnet partitioning. This is in obvious contrast to the incoherent cloud patterns produced from pre-existing detrital cores in other samples (Figure 4e,f). The orientation of the older zircon array is impossible to match with the Taylor et al. (2015b) experimental data on the array plot, even if the REE concentrations were appropriate, the orientation is

negatively sloping, and therefore does not appear to reflect any combination of zircon–garnet partitioning possible from typical mineral REE patterns.

3.2.2 | Crosby nunatak – zircon orthopyroxene partitioning

A second gneiss from Crosby nunatak (Sample 171279/1), having a relatively simple mineral assemblage comprising almost entirely orthopyroxene, K-feldspar and some quartz, contains predominantly *c.* 2850–2700 Ma zircon with a small number of grains extending to a younger age *c.* 2450 Ma (Figure 8c). This sample has no garnet, so the zircon data is plotted against the REE concentrations of the orthopyroxene using the same parameters (Figure 8d).

4 | EVALUATION OF STRAIN MODELLING PARAMETERS

The concave upward shape of the D_{REE}*(zircon–garnet)* traditional REE plot (Figure 1) is the result of the dividing the zircon–melt partition coefficients by the garnet–melt partition coefficients for each element, essentially producing an interference pattern, of which the array plot is a simplified version. The varied position of the D_{REE}*(zircon–garnet)* data on the array plot can be related to the possibility that each zircon experiences minor differences in its local environment, particularly in terms of temperature and composition (*T*-*x*) e.g. being armoured inside another phase, or at times in contact with silicate melt through a different time interval. However the basis for the array must also be compatible with how and why trace elements are incorporated into zircon and garnet.

Rare earth element partition coefficients were calculated for theoretical zircon–garnet pairs using the model of (Blundy and Wood, 1994) across the temperature range 750–1100°C, constrained here by the requirement to produce a match to the 900–1000°C data of Taylor et al. (2015b) on the array plot. The starting point for this theoretical approach is to use the 1000°C zircon parameters from Taylor et al. (2015b), and to assume a relationship between r_0 and E (e.g. Draper and van Westrenen, 2007; van Westrenen and Draper, 2007), which for zircon–melt systems is anchored by the study of Hanchar et al. (2001). Constraints on the values of the strain parameters are drawn from the Taylor et al. (2015b) experimental data, whereby an increase in temperature results in a decrease in R_0, D_0, and E (ideal site radius, ideal partition coefficient, and apparent Young's modulus respectively) for zircon, whilst for garnet there is a concomitant decrease in R_0 and D_0, and a minor increase in E. Given that the 900–950°C experiments of Taylor et al. (2015b) produced M–HREE partition coefficients that overlap within uncertainty, the strain parameters have been chosen to match the modelled and experimental data across the full 900–1000°C range. These multiple constraints—the strain model parameters varying in an experimentally determined manner, and the resultant D_{REE}*(zircon–garnet)* values having to match both the general shape of the traditional REE plot (Figure 9a), and the spread on the array plot (Figure 9b)—result in a set of partition coefficients across the entire granulite facies temperature range at 7 kbar (values for plotting modelled array can be found in Table 1).

The calculated partition coefficients for 750–1100°C have characteristic features on the traditional REE plot, which match those expected from experimental data: concave-up patterns with LREE favouring zircon and the lowest points (i.e. most in favour of garnet) in the M–HREE. Values of approximately 1 for all temperatures occur at an ionic radius of ~1.05 Å, between Eu and Gd. At 1100°C, the HREE favour garnet with D values of ~ 0.4, whilst at 750°C they favour zircon with D values of ~ 3-5,

producing a total spread of D_{HREE}*(zircon–garnet)* of approximately one order of magnitude (Figure 9a). Variation in the strain modelling parameter values with temperature is relatively small in zircon D_0/dT = 0.2 per °C, E/dT = 1 kbar/°C, and R_0/dT = $2x10^{-5}$ per °C. Corresponding variation for garnet are D_0/dT = 0.2 per °C, E/dT = 2 kbar/°C, and R_0/dT = $1.3x10^{-4}$ per °C. All variations have been assumed to be linear, which is unlikely to be the case in nature, especially for parameters such as E at >1000°C, however a linear variation serves here to demonstrate the relative differences between the two minerals.

The REE patterns for the modelled zircon and garnet appear realistic when the D_{REE} values are examined relative to an idealised granite REE composition. Modelled zircon shows flat M–HREE slopes (Figure 9c), typical for metamorphic zircon, covering less than half an order-of-magnitude across the full temperature range, and decreasing in REE content with temperature. Garnet shows a more complex and larger variation, with a more negatively sloping M–HREE pattern at low-*T*, and more positive slopes at high-*T* (Figure 9d). The resultant effect is that garnet MREE such as Gd decrease with temperature, whilst the HREE show the opposite trend but cover less than an order-of-magnitude in HREE. The predicted total REE contents in garnet increase up to ~950–1000°C, and then decrease at higher temperature. This decrease in REE in garnet at temperatures >1000°C matches the previous experimental data of Nicholls and Harris (1980), and may be a genuine phenomenon reflecting a propensity for REE to incorporate into melt at high-*T,* or an artefact of the model fit. Whilst it is possible to create a similar set of modelled partition coefficients with steeply sloping M–HREE in zircon, and flatter, elevated garnet M–HREE, it would require significantly different strain parameters inconsistent with the experimental data, and therefore be almost impossible to satisfy the additional constraint of the array plot.

5. | DISCUSSION

Using the array plot to compare natural samples to experimental data has been demonstrated to be a useful way to evaluate D_{REE}*(zircon–garnet)* equilibrium in high-grade metamorphic rocks. Whilst it may not provide an ultimate answer to petrochronological studies the array approach can, and should, be used in conjunction with textural observations, and other mineral chemistry in order to interpret metamorphic zircon populations. The examples from S. India provide a simple range of possibilities for using the array plot to interpret D_{REE}*(zircon–garnet)* data. The first example (Sample I12-002a – Figure 4) highlights the efficacy of the array plot to evaluating equilibrium zircon–garnet partitioning even in situations where variations in garnet composition are subtle. As a simple, well-constrained example it clearly demonstrates that the metamorphic zircon-garnet relationship forms arrays similar to the experimental data, and that the small shift in garnet composition moves the empirical partitioning data to within uncertainty of the experimental values.

The next example (Sample I11-013 – Figure 5) takes the process a step further, with multiple garnet generations. In this case both the modified garnet 1 rims and garnet 2 give D_{REE} values within uncertainty of the experimental array. This likely indicates that the modification of the prograde garnet 1 rims in the presence of anatectic melt occurred during the growth of peritectic garnet 2, but that the supply/diffusion of HREE was too slow to reach the same equilibrium composition. The better match to the late garnet supports the interpretation that the zircon age again reflects post-peak processes (Taylor et al., 2015a). This sample also highlights that

some datasets appear to spread far beyond the experimentally determined array at 7 kbar, and closer to the 20 kbar experimental data of Rubatto and Hermann (2007) visualised in Figure 3, however a direct comparison with this dataset would also require a justification regarding the relevant pressure or garnet composition.

The third Achankovil Zone example (Sample I11-014 – Figure 6) demonstrates the array plot's ability to show disequilibrium patterns even where the traditional REE plot suggests D_{REE}*(zircon–garnet)* equilibrium, as suggested in the original study (Taylor et al., 2015a). This apparent lack of clear chemical equilibrium fits with the ages and field relationships, where the texturally late, cross-cutting granite sheet has a zircon age older than the metasedimentary rock into which it intruded. One explanation of these data is that the emplacement of an externally generated melt into the crust stimulated the rapid growth/recrystallization of zircon (e.g. Harley and Nandakumar, 2014), whilst the host garnet–cordierite gneiss still contained its own partial melt with a lower solidus than the granite sheet. This scenario may result in zircon ages that are closer to the timing of peak metamorphism than the post-peak melt crystallization ages seen in the host gneiss. Resulting in the slightly counter intuitive approach of highlighting the use of metamorphic zircon ages that are not necessarily in equilibrium with associated garnet. It may be that the peritectic garnet formed within the melt at source and was transported with it, whereas the zircon may be a mix of grains that formed/modified during transit or from rapid crystallization at shallower levels.

The two samples from the Crosby nunatak in Enderby land provide an intriguing insight into the directions the array plot approach could be taken, identifying possible equilibrium partitioning signature of major minerals for which there are no experimental data. The garnet-bearing gneiss (Sample 171279/3) demonstrated both a positive, zircon-garnet array slope for one zircon population, and a distinctly negative array for the older zircon population. Previous examples suggest that if detrital zircon formed in a host with no major HREE-bearing phase, as assumed for Figure 4e,f, the result is scatter on the array plot. In contrast the coherent, negatively sloping array in Figure 8b is likely the result of partitioning between zircon and HREE-bearing phase that is not garnet.

Whilst there are no experimental D_{REE}*(zircon–orthopyroxene)* data with which to compare, it is notable that the resultant array for the orthopyroxene gneiss (Sample 171279/1) is negatively sloping. If this pattern on the array plot is indeed a defining feature of zircon–orthopyroxene trace element equilibrium, it suggests that the older, steep HREE zircon in the garnet-bearing sample 171279/3 was in equilibrium with orthopyroxene that is no longer present in the rock. Ti-in-zircon shows maximum values in the older zircon for both samples in the range of 65-91 ppm, whilst the *c.* 2451 Ma zircon maximum values are 44 ppm, corresponding to 958–1006°C and 910°C respectively. These temperatures suggest the older zircon reflects either a metamorphic event at a higher-*T*, or potentially have grown in an anhydrous, orthopyroxene-bearing high-*T* magma.

The sensitivity of the array plot enables further inferences to be made into existing studies, beyond the interpretations of those authors at the time. For example, the Napier Complex UHT study of Hokada and Harley (2004) (Figure 9e) presented a number of possible scenarios regarding the timing of zircon growth and resultant flat D_{HREE}*(zircon–garnet)* profiles in a sample with a minimum temperature of 950°C at 8 kbar. Comparing their analyses to the modelled array plot suggests that unlike the

original interpretation, the garnet cores are in equilibrium with the zircon rims, and that the late loss of MREE in garnet is therefore more likely related to the growth of late, interstitial monazite identified in the study. The effect of this monazite growth shifts the array plot data to the left, i.e. a change in partitioning slope without changing the D_{HREE}. It is also notable that the D_{REE}*(zircon–garnet)* falls in the 1000–1050°C range of the modelled array, which is a reasonable temperature estimate for the Napier Complex. The timing of monazite growth relative to zircon may have a key role in variations observed with the array approach, particularly in regions such as S. India where it is ubiquitous.

The study of Whitehouse and Platt (2003) (Figure 9f) demonstrates the variation in D_{REE}*(zircon–garnet)* with the modification of the garnet HREE composition during metamorphism at 750–800°C and ~4 kbar. As the analytical traverse goes from garnet core REE values towards the garnet rim partitioning data becomes coincident with the modelled array, agreeing with the original interpretation. However, even the lowest HREE rim values clusters the majority of the data around a modelled temperature of ~950°C, higher than that based on the petrological interpretation of the rocks studied. However, this study only had partial REE data (crucially no Yb) for the extreme rim of the zoned garnet, and therefore the array approach was not able to be applied using the portion of the garnet most likely to be in equilibrium with the garnet, but the available data suggests it was approaching equilibrium based on the experimental array. This indeed highlights another frailty in the use of REE in such studies, if the necessary mineral zones are to small to target with available analytical techniques.

Using the most important parameters to define partitioning relationships could also provide benefits when assessing whether other accessory minerals—e.g. HREE in monazite or LREE in apatite—were in equilibrium with silicate minerals. Currently, in the absence of experimentally derived REE partitioning data these accessory mineral relationships can only be determined by identifying trends based on well-characterised natural examples, however even this may provide useful insights.

The strain modelling approach described here, which predicts D_{REE}*(zircon–garnet)* across a range of temperatures, is fraught with uncertainty due to the number of parameters used to fit the data. Reconciling both the array plot and traditional REE plot with experimentally-derived data reduces the uncertainty in the parameter fits, increasing the likelihood that the predicted partition coefficients have some value, however there are still caveats highlighted by this approach. The fits for garnet–melt parameters used here are not based on any previously determined models (e.g. van Westrenen et al., 2001; van Westrenen and Draper, 2007), but are only empirically modified to produce a satisfactory fit. The slope parameter may not be the best description of the D_{REE}*(zircon–garnet)* values, for example 'D_{Yb}/D_{Dy}' may be more descriptive in case studies where there is a larger degree of inflection/curvature through the HREE. The 20 kbar dataset of Rubatto and Hermann (2007), which covers a large range in temperature and composition, highlights the lack of experimental data to which empirical data can be correctly fitted. It is impossible to say with the currently available data whether any fit of natural examples to experimental data should be based on temperature, pressure or composition. To benefit fully from the sensitivity of this array plot approach, it is essential that further experimental data be acquired to evaluate the importance of these variables.

ACKNOWLEDGEMENTS

Studies on the Southern Granulite Terrane and Enderby Land were funded by the Australian Research Council DECRA (DE120103067) project awarded to C. Clark. The authors thank H. Marschall, and a very thorough anonymous reviewer for their comments that greatly improved the final manuscript. We would also like to thank M. Brown for his editorial handling.

REFERENCES

Ague, J.J., & Baxter, E.F., 2007. Brief thermal pulses during mountain building recorded by Sr diffusion in apatite and multicomponent diffusion in garnet. Earth and Planetary Science Letters, 261(3-4): 500-516.

Ashwal, L.D., Tucker, R.D., & Zinner, E.K., 1999. Slow cooling of deep crustal granulites and Pb-loss in zircon. Geochimica et Cosmochimica Acta, 63(18): 2839-2851.

Black, L., Williams, I., & Compston, W., 1986. Four zircon ages from one rock: the history of a 3930 Ma-old granulite from Mount Sones, Enderby Land, Antarctica. Contributions to Mineralogy and Petrology, 94(4): 427-437.

Blereau, E. et al., 2016. Constraints on the timing and conditions of high-grade metamorphism, charnockite formation, and fluid-rock interaction in the Trivandrum Block, southern India. Journal of Metamorphic Geology: 527-549.

Blundy, J., & Wood, B., 1994. Prediction of crystal-melt partition coefficients from elastic moduli. Nature, 372(6505): 452-454.

Braun, I., & Bröcker, M., 2004. Monazite dating of granitic gneisses and leucogranites from the Kerala Khondalite Belt, southern India: Implications for Late Proterozoic crustal evolution in East Gondwana. International Journal of Earth Sciences, 93(1): 13-22.

Buick, I.S., Hermann, J., Williams, I.S., Gibson, R.L., & Rubatto, D., 2006. A SHRIMP U-Pb and LA-ICP-MS trace element study of the petrogenesis of garnet–cordierite-orthoamphibole gneisses from the Central Zone of the Limpopo Belt, South Africa. Lithos, 88(1-4): 150-172.

Cherniak, D.J., Hanchar, J.M., & Watson, E.B., 1997. Rare-earth diffusion in zircon. Chemical Geology, 134(4): 289-301.

Cherniak, D.J., & Watson, E.B., 2001. Pb diffusion in zircon. Chemical Geology, 172(1-2): 5-24.

Cherniak, D.J., & Watson, E.B., 2003. Diffusion in zircon. In: Hanchar JM, Hoskin, PWO (eds) Zircon. Reviews in Mineralogy 53, Mineralogical Society of America: 113-143.

Cherniak, D.J., & Watson, E.B., 2007. Ti diffusion in zircon. Chemical Geology, 242(3-4): 473-486.

Clark, C., Collins, A.S., Santosh, M., Taylor, R., & Wade, B.P., 2009. The P-T-t architecture of a Gondwanan suture: REE, U-Pb and Ti-in-zircon thermometric constraints from the Palghat Cauvery shear system, South India. Precambrian Research, 174(1-2): 129-144.

Clark, C. et al., 2015. Hot orogens and supercontinent amalgamation: A Gondwanan example from southern India. Gondwana Research, 28(4): 1310-1328.

Collins, A.S., Clark, C., & Plavsa, D., 2014. Peninsular India in Gondwana: The tectonothermal evolution of the Southern Granulite Terrain and its Gondwanan counterparts. Gondwana Research, 25(1): 190-203.

Corfu, F., Hanchar, J.M., Hoskin, P.W.O., & Kinny, P., 2003. Atlas of zircon textures.

Dempster, T.J., Symon, S., & Chung, P., 2017. Intergranular diffusion rates from the analysis of garnet surfaces: implications for metamorphic equilibration. Journal of Metamorphic Geology: n/a-n/a.

Draper, D.S., & van Westrenen, W., 2007. Quantifying garnet-melt trace element partitioning using lattice-strain theory: Assessment of statistically significant controls and a new predictive model. Contributions to Mineralogy and Petrology, 154(6): 731-746.

Estrada-Carmona, J., Solari, L.A., & Ortega-Obregón, C., 2016. Petrochronology of the migmatization event of the Xolapa Complex, Mexico, microchemistry and equilibrium growth of zircon and garnet. International Geology Review, 58(11): 1382-1397.

Fonarev, V.I., Konilov, A.N., & Santosh, M., 2000. Multistage Metamorphic Evolution of the Trivandrum Granulite Block, Southern India. Gondwana Research, 3(3): 293-314.

Fornelli, A., Langone, A., Micheletti, F., Pascazio, A., & Piccarreta, G., 2014. The role of trace element partitioning between garnet, zircon and orthopyroxene on the interpretation of zircon U–Pb ages: an example from high-grade basement in Calabria (Southern Italy). International Journal of Earth Sciences, 103(2): 487-507.

Gordon, S.M., Whitney, D.L., Teyssier, C., Fossen, H., & Kylander-Clark, A., 2016. Geochronology and geochemistry of zircon from the northern Western Gneiss Region: Insights into the Caledonian tectonic history of western Norway. Lithos, 246: 134-148.

Hanchar, J.M. et al., 2001. Rare earth elements in synthetic zircon: Part 1. Synthesis, and rare earth element and phosphorus doping. American Mineralogist, 86(5-6): 667-680.

Harley, S., Black, L., 1987. The Archaean geological evolution of Enderby Land, Antarctica. Geological Society, London, Special Publications, 27(1): 285-296.

Harley, S.L., 1985. Garnet–orthopyroxene bearing granulites from enderby land, Antarctica: Metamorphic pressure temperature-time evolution of the archaean napier complex. Journal of Petrology, 26(4): 819-856.

Harley, S.L., & Black, L.P., 1997. A revised Archaean chronology for the Napier Complex, Enderby Land, from SHRIMP ion-microprobe studies. Antarctic Science, 9(1): 74-91.

Harley, S.L., & Kelly, N.M., 2007. The impact of zircon-garnet REE distribution data on the interpretation of zircon U-Pb ages in complex high-grade terrains: An example from the Rauer Islands, East Antarctica. Chemical Geology, 241(1-2): 62-87.

Harley, S.L., Kelly, N.M., & Moller, A., 2007. Zircon behaviour and the thermal histories of mountain chains. Elements, 3(1): 25-30.

Harley, S.L., Kinny, P., Snape, I., & Black, L.P., 2001. Zircon chemistry and the definition of events in Archean granulite terrains. In: Fourth International Archean Symposium, Extended Abstract Volume, AGSO Geoscience Australia Record, 2001/37: 511-513.

Harley, S.L., & Nandakumar, V., 2014. Accessory Mineral Behaviour in Granulite Migmatites: a Case Study from the Kerala Khondalite Belt, India. Journal of Petrology, 55(10): 1965-2002.

Harley, S.L., & Nandakumar, V., 2016. New evidence for Palaeoproterozoic high grade metamorphism in the Trivandrum Block, Southern India. Precambrian Research, 280: 120-138.

Hermann, J., & Rubatto, D., 2003. Relating zircon and monazite domains to garnet growth zones: Age and duration of granulite facies metamorphism in the Val Malenco lower crust. Journal of Metamorphic Geology, 21(9): 833-852.

Hermann, J., & Rubatto, D., 2009. Accessory phase control on the trace element signature of sediment melts in subduction zones. Chemical Geology, 265(3-4): 512-526.

Hokada, T.,& Harley, S.L., 2004. Zircon growth in UHT leucosome: Constraints from zircon-garnet rare earth elements (REE) relations in Napier Complex, East Antarctica. Journal of Mineralogical and Petrological Sciences, 99(4): 180-190.

Hokada, T., Misawa, K., Yokoyama, K., Shiraishi, K., & Yamaguchi, A., 2004. SHRIMP and electron microprobe chronology of UHT metamorphism in the Napier Complex, East Antarctica: implications for zircon growth at > 1,000 degrees C. Contributions to Mineralogy and Petrology, 147(1): 1-20.

Johnson, T.E., Clark, C., Taylor, R.J.M., Santosh, M., & Collins, A.S., 2015. Prograde and retrograde growth of monazite in migmatites: an example from the Nagercoil Block, southern India. Geoscience Frontiers, 6(3): 373-387.

Kelly, N.M., & Harley, S.L., 2005. An integrated microtextural and chemical approach to zircon geochronology: Refining the Archaean history of the Napier Complex, east Antarctica. Contributions to Mineralogy and Petrology, 149(1): 57-84.

Kelsey, D.E., Clark, C., & Hand, M., 2008. Thermobarometric modelling of zircon and monazite growth in melt-bearing systems: Examples using model metapelitic and metapsammitic granulites. Journal of Metamorphic Geology, 26(2): 199-212.

Korhonen, F.J., Clark, C., Brown, M., Bhattacharya, S., & Taylor, R., 2013. How long-lived is ultrahigh temperature (UHT) metamorphism? Constraints from zircon and monazite geochronology in the Eastern Ghats orogenic belt, India. Precambrian Research, 234: 322-350.

Korhonen, F.J., Clark, C., Brown, M., & Taylor, R.J.M., 2014. Taking the temperature of Earth's hottest crust. Earth and Planetary Science Letters, 408: 341-354.

Kotková, J., & Harley, S.L., 2010. Anatexis during high-pressure crustal metamorphism: Evidence from garnet-whole-rock REE relationships and zircon-rutile Ti-Zr thermometry in leucogranulites from the Bohemian Massif. Journal of Petrology, 51(10): 1967-2001.

Kusiak, M.A. et al., 2013a. Changes in zircon chemistry during Archean UHT metamorphism in the Napier Complex, Antarctica. American Journal of Science, 313(9): 933-967.

Kusiak, M.A., Whitehouse, M.J., Wilde, S.A., Nemchin, A.A., & Clark, C., 2013b. Mobilization of radiogenic Pb in zircon revealed by ion imaging: Implications for early Earth geochronology. Geology, 41(3): 291-294.

Kylander-Clark, A.R.C., Hacker, B.R., & Cottle, J.M., 2013. Laser-ablation split-stream ICP petrochronology. Chemical Geology, 345(0): 99-112.

Nandakumar, V., & Harley, S.L., 2000. A reappraisal of the pressure-temperature path of granulites from the Kerala Khondalite Belt, Southern India. Journal of Geology, 108(6): 687-703.

Nicholls, I.A., & Harris, K.L., 1980. Experimental rare earth element partition coefficients for garnet, clinopyroxene and amphibole coexisting with andesitic and basaltic liquids. Geochimica et Cosmochimica Acta, 44(2): 287-308.

Pyle, J.M., & Spear, F.S., 2003. Yttrium zoning in garnet: Coupling of major and accessory phases during metamorphic reactions. American Mineralogist, 88(4): 708.

Raith, M. et al., 2016. Element Mobility and Behaviour of Zircon during HT Metasomatism of Ferroan Basic Granulite at Ayyarmalai, South India: Evidence for Polyphase Neoarchaean Crustal Growth and Multiple Metamorphism in the Northeastern Madurai Province. Journal of Petrology, 57(9): 1729-1774.

Roberts, M.P., & Finger, F., 1997. Do U-Pb zircon ages from granulites reflect peak metamorphic conditions? Geology, 25(4): 319-322.

Rubatto, D., 2002. Zircon trace element geochemistry: Partitioning with garnet and the link between U-Pb ages and metamorphism. Chemical Geology, 184(1-2): 123-138.

Rubatto, D., & Hermann, J., 2007. Experimental zircon/melt and zircon/garnet trace element partitioning and implications for the geochronology of crustal rocks. Chemical Geology, 241(1-2): 38-61.

Rubatto, D., Williams, I.S., & Buick, I.S., 2001. Zircon and monazite response to prograde metamorphism in the Reynolds Range, central Australia. Contributions to Mineralogy and Petrology, 140(4): 458-468.

Santosh, M. et al., 2006a. The timing of ultrahigh-temperature metamorphism in Southern India: U-Th-Pb electron microprobe ages from zircon and monazite in sapphirine-bearing granulites. Gondwana Research, 10(1-2): 128-155.

Santosh, M., Morimoto, T., & Tsutsumi, Y., 2006b. Geochronology of the khondalite belt of Trivandrum Block, Southern India: Electron probe ages and implications for Gondwana tectonics. Gondwana Research, 9(3): 261-278.

Štípská, P., Powell, R., Hacker, B., Holder, R., & Kylander-Clark, A., 2016. Uncoupled U/Pb and REE response in zircon during the transformation of eclogite to mafic and intermediate granulite (Blanský les, Bohemian Massif). Journal of Metamorphic Geology, 34(6): 551-572.

Tadokoro, H., Tsunogae, T., & Santosh, M., 2008. Metamorphic P-T path of the eastern Trivandrum Granulite Block, southern India: Implications for regional correlation of lower crustal fragments. Journal of Mineralogical and Petrological Sciences, 103(4): 279-284.

Taylor, R.J.M. et al., 2014. Post-peak, fluid-mediated modification of granulite facies zircon and monazite in the Trivandrum Block, southern India. Contributions to Mineralogy and Petrology, 168(2): 1-17.

Taylor, R.J.M., Clark, C., Johnson, T.E., Santosh, M., & Collins, A.S., 2015a. Unravelling the complexities in high-grade rocks using multiple techniques – the Achankovil Zone of southern India Contributions to Mineralogy & Petrology, 169(5): 1-19.

Taylor, R.J.M. et al., 2015b. Experimental determination of REE partition coefficients between zircon, garnet and melt: A key to understanding high-T crustal processes. Journal of Metamorphic Geology, 33(3): 231-248.

Taylor, R.J.M., Kirkland, C.L., & Clark, C., 2016. Accessories after the facts: Constraining the timing, duration and conditions of high-temperature metamorphic processes. Lithos, 264: 239-257.

Timms, N.E. et al., 2011. Relationship among titanium, rare earth elements, U-Pb ages and deformation microstructures in zircon: Implications for Ti-in-zircon thermometry. Chemical Geology, 280(1-2): 33-46.

van Westrenen, W., Blundy, J.D., & Wood, B.J., 2001. High field strength element/rare earth element fractionation during partial melting in the presence of garnet: Implications for identification of mantle heterogeneities. Geochemistry, Geophysics, Geosystems, 2(7): n/a-n/a.

van Westrenen, W., & Draper, D.S., 2007. Quantifying garnet-melt trace element partitioning using lattice-strain theory: New crystal-chemical and thermodynamic constraints. Contributions to Mineralogy and Petrology, 154(6): 717-730.

Watson, E.B., & Baxter, E.F., 2007. Diffusion in solid-Earth systems. Earth and Planetary Science Letters, 253(3-4): 307-327.

Watt, G.R., & Harley, S.L., 1993. Accessory phase controls on the geochemistry of crustal melts and restites produced during water-undersaturated partial melting. Contributions to Mineralogy and Petrology, 114(4): 550-566.

Whitehouse, M.J., & Platt, J.P., 2003. Dating high-grade metamorphism - Constraints from rare-earth elements in zircon and garnet. Contributions to Mineralogy and Petrology, 145(1): 61-74.

Yakymchuk, C. et al., 2015. Decoding polyphase migmatites using geochronology and phase equilibria modelling. Journal of Metamorphic Geology, 33(2): 203-230.

SUPPORTING INFORMATION

Additional Supporting Information may be found online in the supporting information tab for this article.

Received 2 February 2017; revision accepted 12 April 2017.

Table S1. Kullapara, S. India metapelite (sillimanite gneiss) – a) Zircon U-Pb and trace element data for Figure 7; b) Garnet REE data for Figure 7.

Table S2. Crosby Nunatak, Enderby Land – a) U-Pb and trace element LASS data (sample 171279/3) for Figures 7 and 8; b) Garnet and Opx trace element data (sample 171279/3) for Figures 7 and 8

Figure captions

Figure 1. Experimental data from Rubatto and Hermann (2007) and Taylor et al. (2015b) for D_{REE}*(zircon–garnet*) in granitic melt, as displayed on a traditional REE plot. These two studies, at 20 kbar and 7 kbar respectively, provide the entire current experimental framework by which zircon–garnet equilibrium REE partitioning is evaluated.

Figure 2. A) Theoretical variations in M–HREE distribution between zircon and garnet on a spider plot. B) Schematic representations of the same partitioning relationships on the array plot showing that, depending on the relationship between the slope and HREE parameters, different possible relationships may produce anything from vertical to horizontal arrays.

Figure 3. The experimental data from Rubatto and Hermann (2007) and Taylor et al. (2015b) (strain modelled) as they appears on the array plot . The data show a positive correlation, i.e. covariance, between the slope parameter, $\log(D_{Yb}/D_{Gd})$, and the HREE parameter $\log(D_{Yb})$, with the lowest values in each case being from the highest temperature experiments.

Figure 4. Empirical data from the garnet–orthopyroxene gneiss of Taylor et al. (2015a) from the Achankovil Zone, southern India. A) Zircon REE data. B) Garnet REE data. C) Traditional REE plot showing D_{REE}(*zircon–garnet*) for all zircon against garnet cores. D) Traditional REE plot showing D_{REE}(*zircon–garnet*) for all zircon against garnet rims. E) Array plot showing D_{REE}(*zircon–garnet*) for all zircon against average garnet cores. F) Array plot showing D_{REE}(*zircon–garnet*) for all zircon against average garnet rims. Array plot shows zircon equilibrium with garnet rims based on match to 7 kbar experimental data.

Figure 5. Empirical data from the garnet–cordierite gneiss of Taylor et al. (2015a) from the Achankovil Zone, southern India. A) Zircon REE data. B) Garnet REE data. C) Array plot showing D_{REE}(*zircon–garnet*) for all zircon against garnet 1 rims. D) Array plot showing D_{REE}(*zircon–garnet*) for all zircon against garnet 2. Array plot shows zircon equilibrium with garnet 2. Garnet one rim composition is related to garnet 2 formation.

Figure 6. Empirical data from the garnet-bearing granite of Taylor et al. (2015a) from the Achankovil Zone, southern India. A) Zircon REE data. B) Garnet REE data. C) Traditional REE plot showing D_{REE}(*zircon–garnet*) for all zircon against garnet rims. D) Array plot showing D_{REE}(*zircon–garnet*) for all zircon against garnet. Array plot suggest no equilibrium signature between zircon and garnet.

Figure 7. Empirical data from Kullapara quarry, Trivandrum Block, southern India (See Table SA for all data). A) Concordia diagram showing all analyses of metamorphic zircon rims for Sample I11-002. U–Pb data show a continuous spread of ages spanning almost 100 Ma. B) Zircon REE data. C) Garnet REE data. D) Array plot showing D_{REE}(*zircon–garnet*) the position of all zircon relative to the three garnet compositions. Numbers on are axes relevant to lowest REE garnet composition. All zircon is in equilibrium with some garnet in the rock.

Figure 8. Empirical data from Crosby nunatak garnet-bearing gneiss (sample 171279/3), and orthopyroxene-bearing gneiss (171279-1), Enderby Land, east Antarctica (See Table S2 for all data). A) Concordia diagram showing U–Pb data for Sample 171279/3. Data show a main population at c. 2.4 Ga with predominantly flat HREE slopes (Yb_N/Gd_N), and a continuous spread of ages up to c. 2.8 Ga show steeper HREE slopes. B) Array plot shows a positive garnet trend for c. 2.4 Ga zircon, but a negative slope for older zircon. C) Concordia diagram showing U–Pb data for Sample 171279/1. Data show a main population at c. 2.8 Ga, with a small number of analyses extending to younger ages, all zircon show positively sloping HREE patterns B) Array plot for D_{REE}(*zircon–orthopyroxene*) has a negative slope, suggesting the 2.8 Ga grains in the previous sample stabilised with a pre-existing, orthopyroxene-bearing assemblage.

Figure 9. Predicted, strain modelled D_{REE}(*zircon–garnet*) values for 750–1100°C using the array plot as an additional constraint. Model values show an order of magnitude variation for HREE partitioning over the 350°C range using the 7 kbar experimental data of Taylor et al. (2015b). To produce the predicted partition coefficients the model must approximate the shape of A) the traditional REE plot, and B) the array plot. C) Modelled zircon REE concentrations produced from the lattice strain model applied to the array plot. D) Modelled garnet REE concentrations produced from the lattice strain model applied to the array plot. Plots E) and F) demonstrate the applicability of the array plot to classic studies of REE partitioning. E) Hokada and Harley (2004) UHT study from Enderby Land leucosomes shows that late monazite growth has shifted the D_{REE}(*zircon–garnet*) values away from equilibrium. F) The Whitehouse and Platt study of the Betic Cordillera shows that the modification of garnet during decompression and partial melting has resulted in a D_{REE}(*zircon–garnet*) signature close to equilibrium with the melt-related zircon rims.

Table 1. Values used for creating the experimental data array. A) Taylor et al. (2015b) 900–1000°C data from Figure 3 values used are those produced by lattice strain modelling. B) 750–1100°C data calculated for Figure 9b by extrapolating the experimental data to higher and lower temperatures, by constraining the lattice strain parameters to the array plot.

Table 1 - D(zircon/garnet) data for plotting

A) Experimental D(zircon/garnet) data - Taylor *et al*., (2015)				
T (°C)	**log(Dslope)**	**±**	**logD(Yb)**	**±**
1000	-0.20	0.10	-0.35	0.08
1000	-0.10	0.04	-0.21	0.03
950	0.14	0.02	-0.003	0.0003
950	0.11	0.02	-0.02	0.00
950	0.14	0.03	0.08	0.01
900	0.09	0.02	-0.16	0.05

*uncertainties are calculated from 95% confidence of Taylor *et a*l., (2015)

B) Lattice strain model D(zircon/garnet) constrained by array *- (Figure 10d)*		
T (°C)	**log(Dslope)**	**logD(Yb)**
1100	-0.42	-0.46
1050	-0.30	-0.34
1000	-0.16	-0.22
950	-0.02	-0.09
900	0.12	0.05
850	0.28	0.20
800	0.44	0.38
750	0.62	0.59

Figure 1

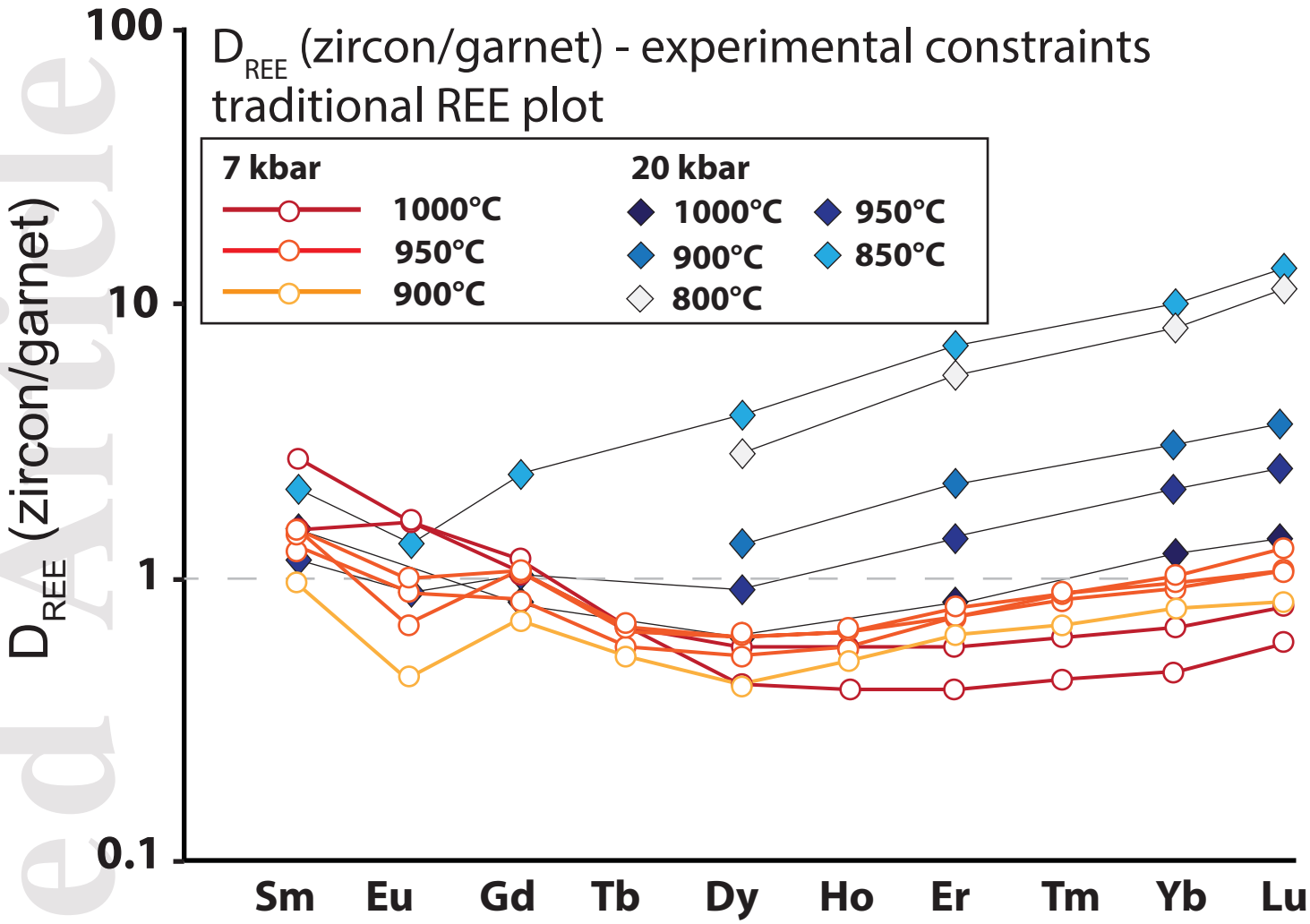

Figure 2

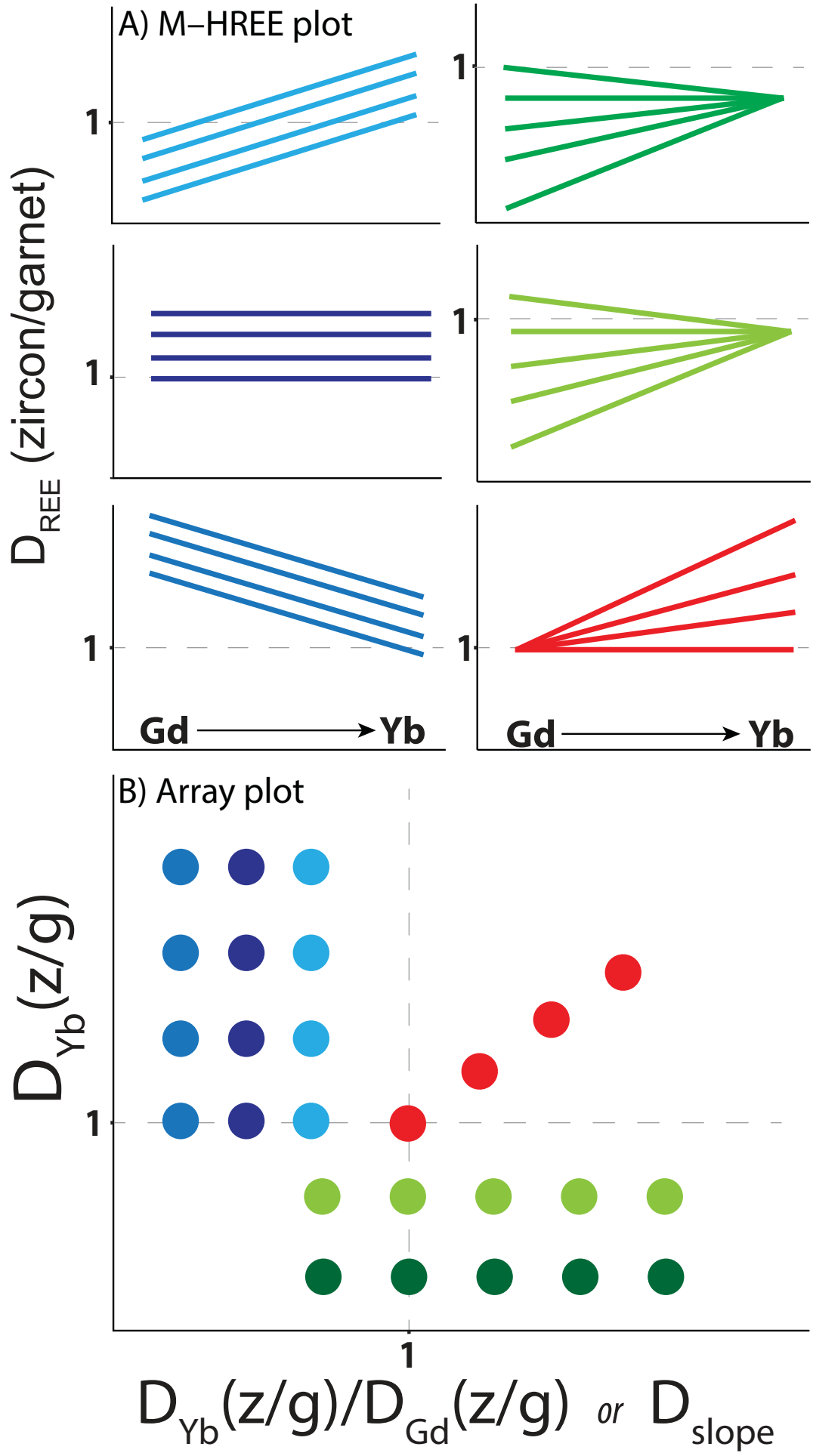

Figure 3

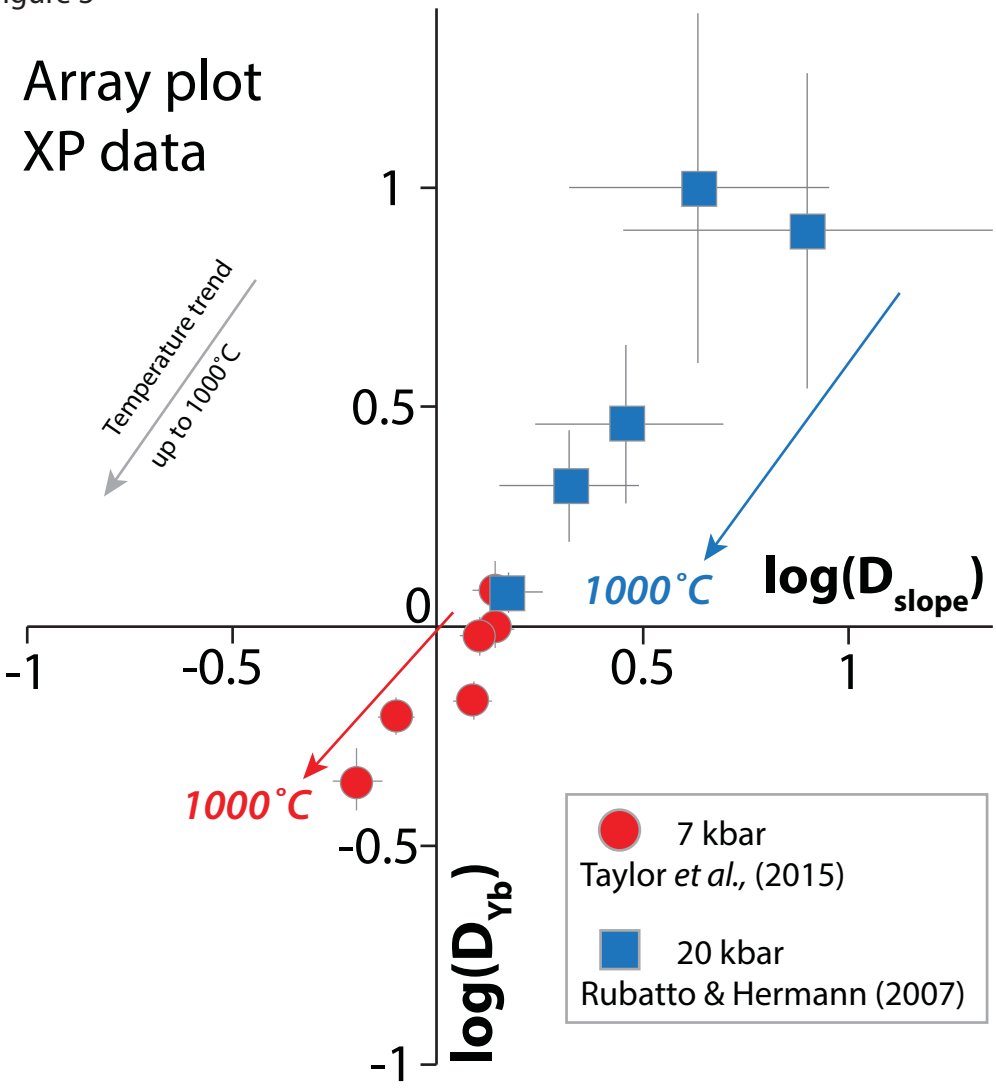

Figure 4

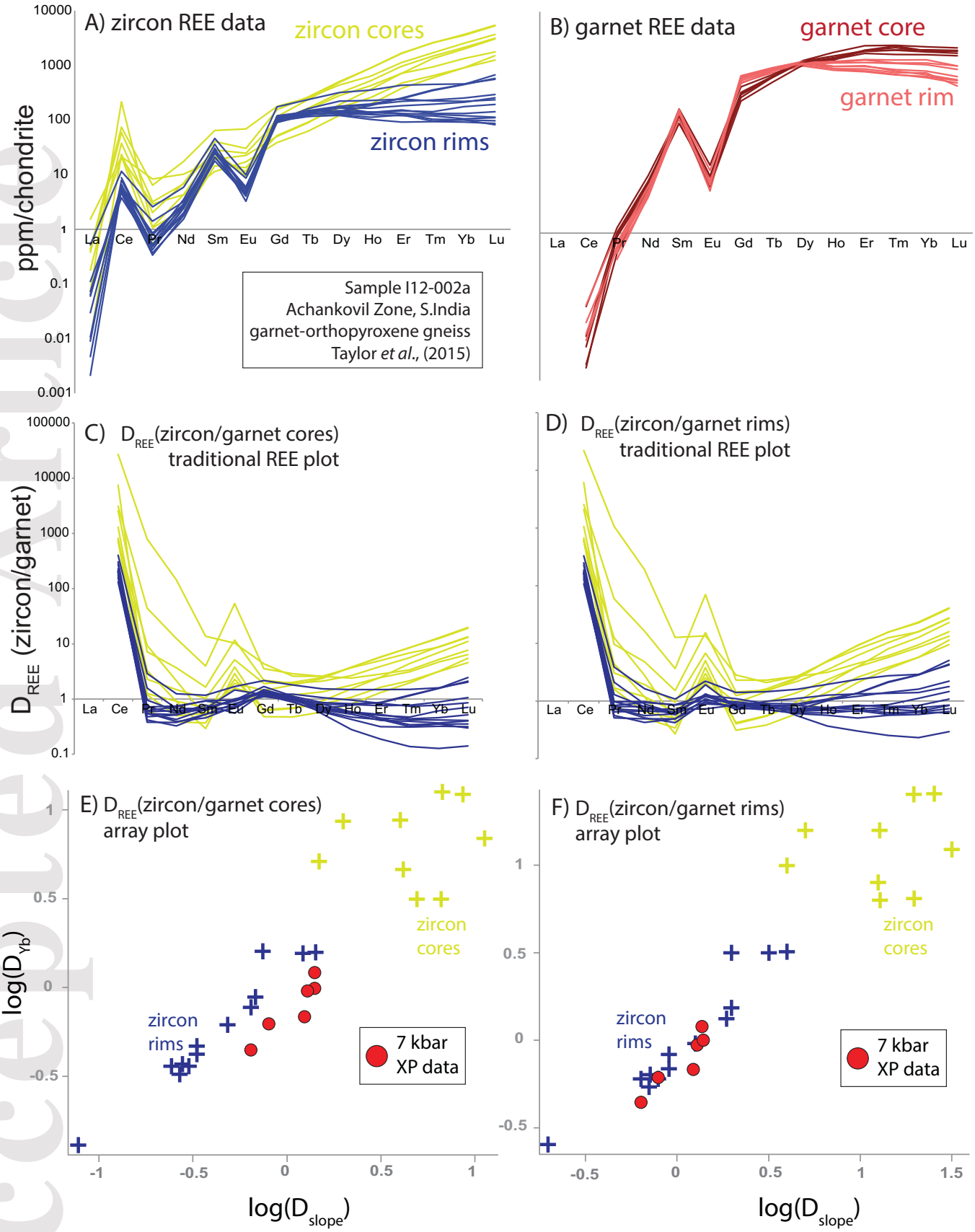

Figure 5

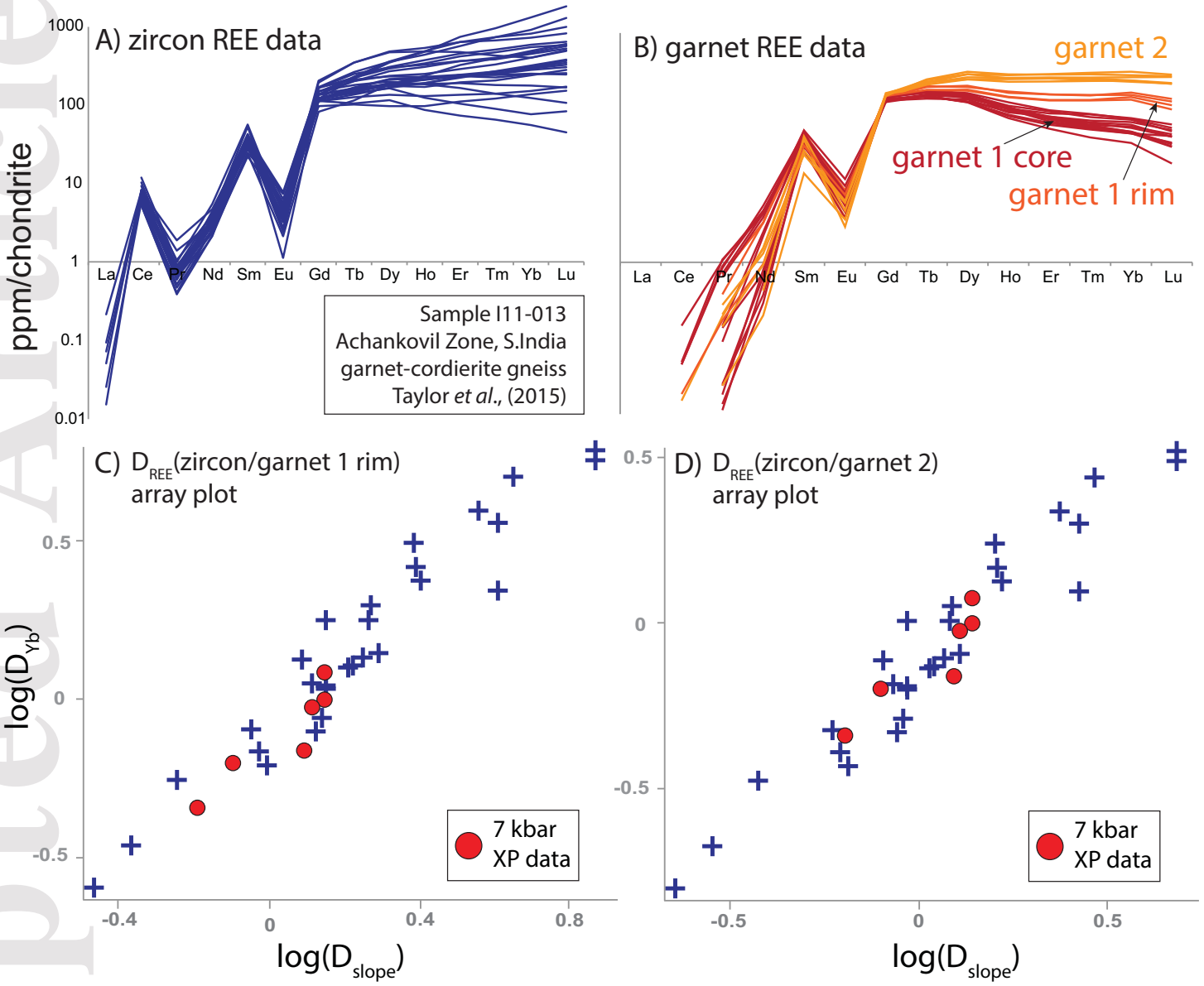

Figure 6

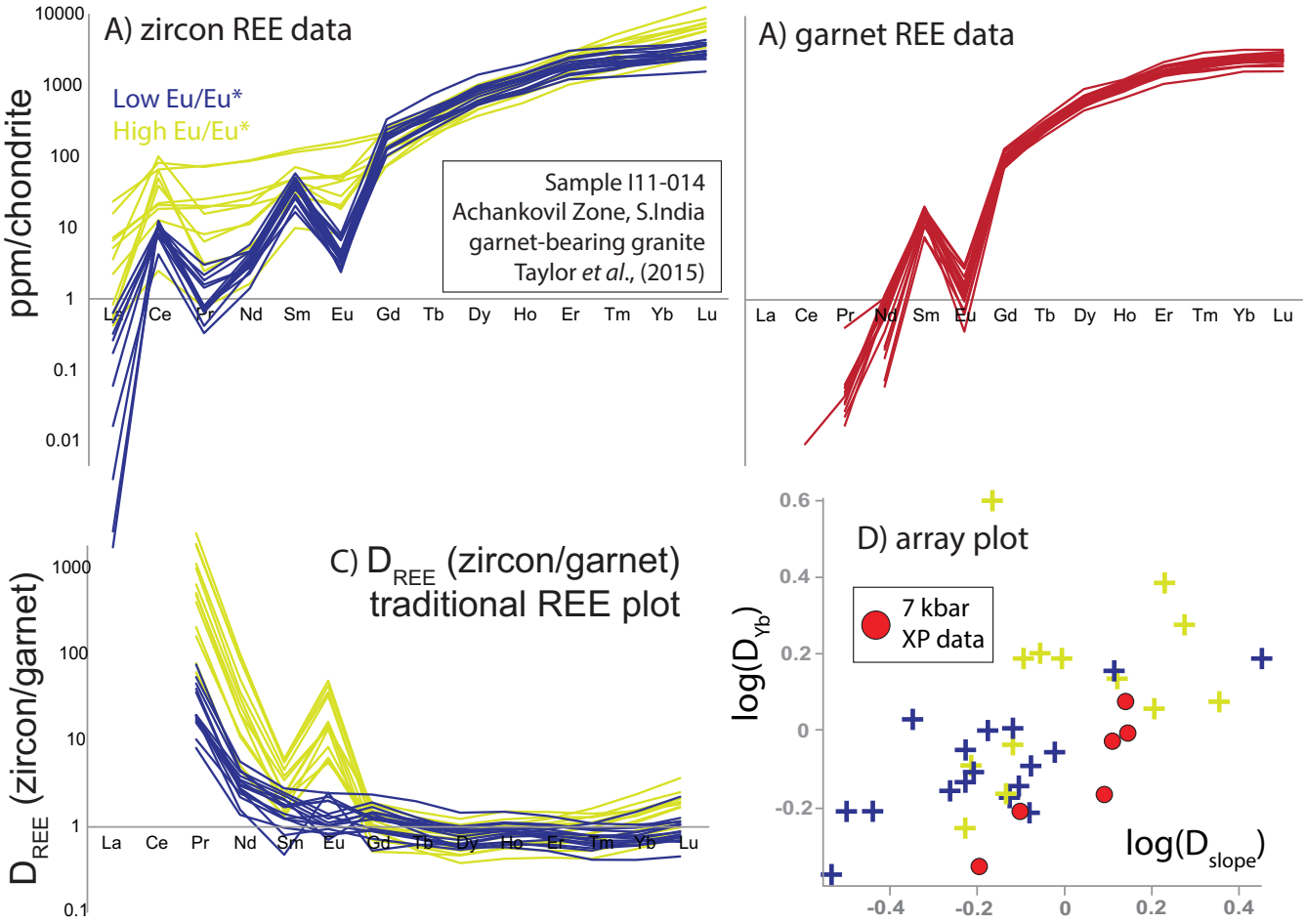

Figure 7

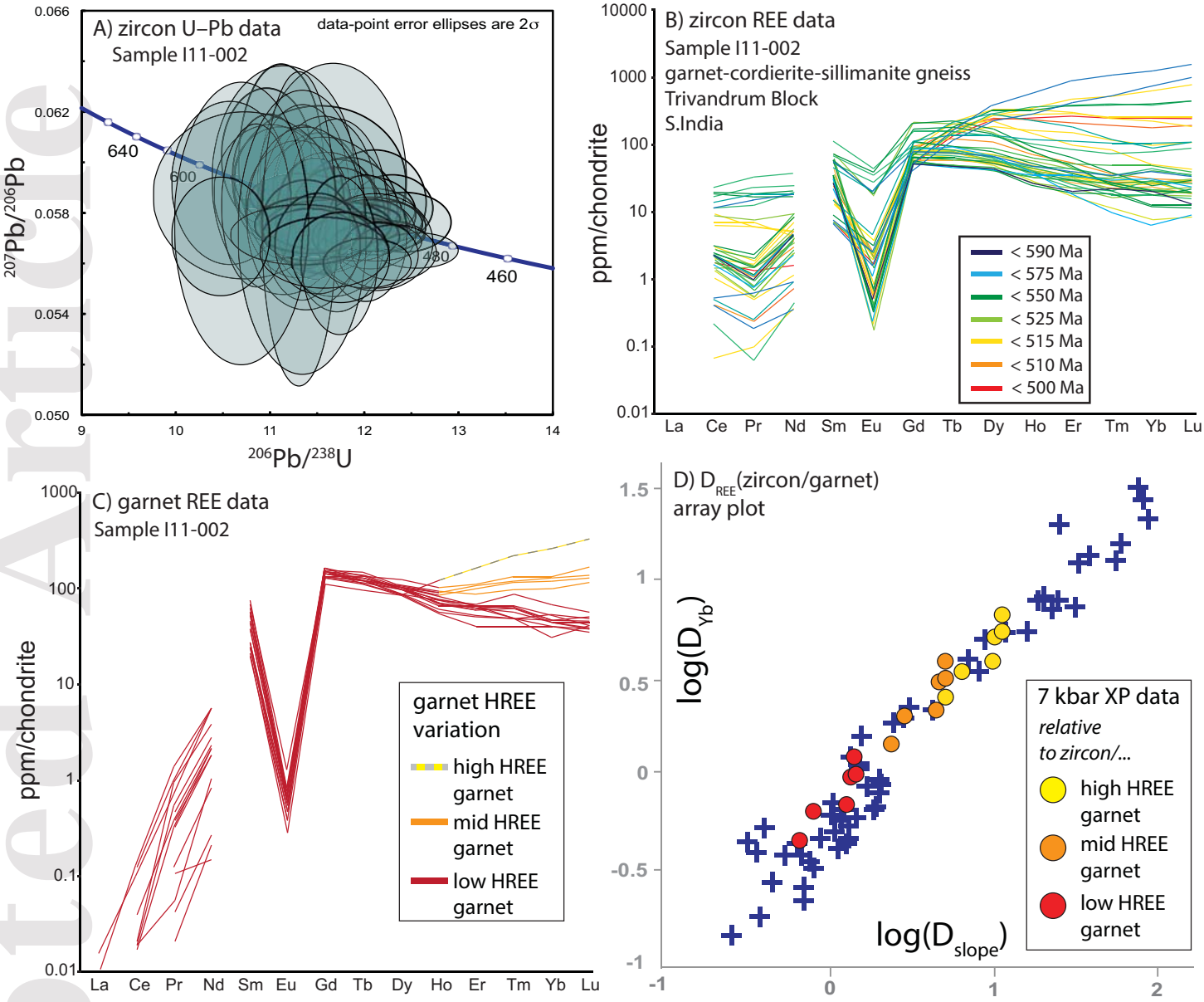

Figure 8

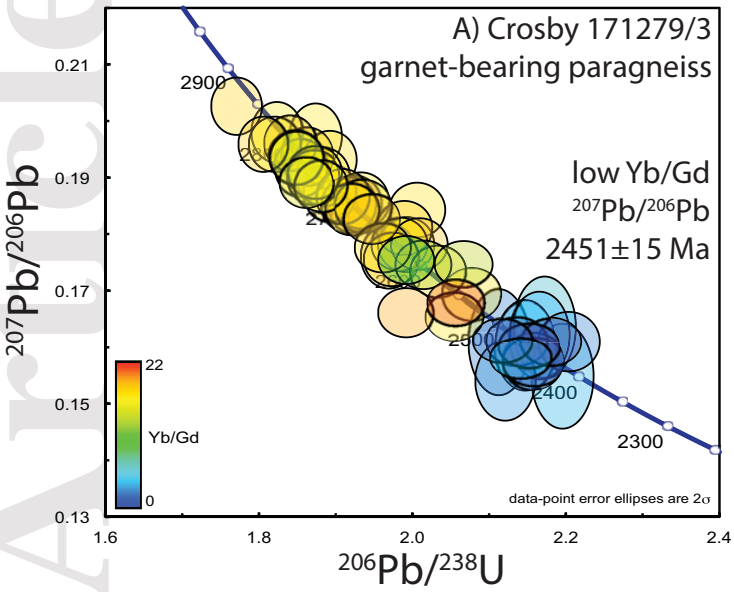

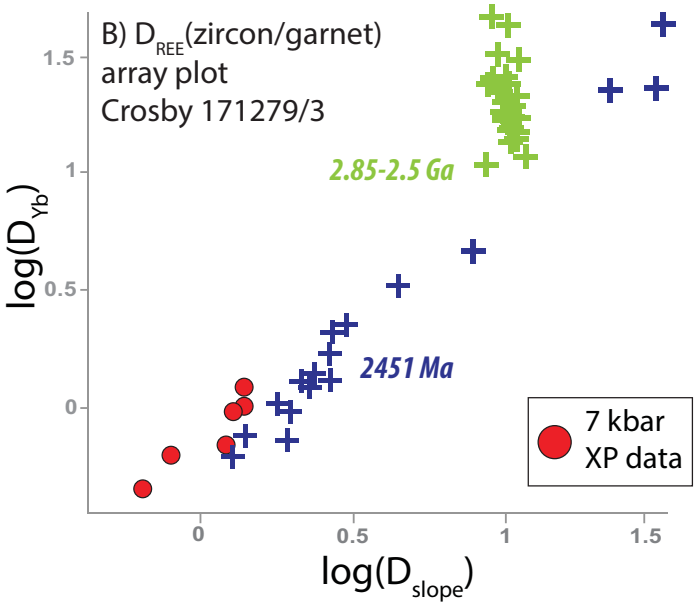

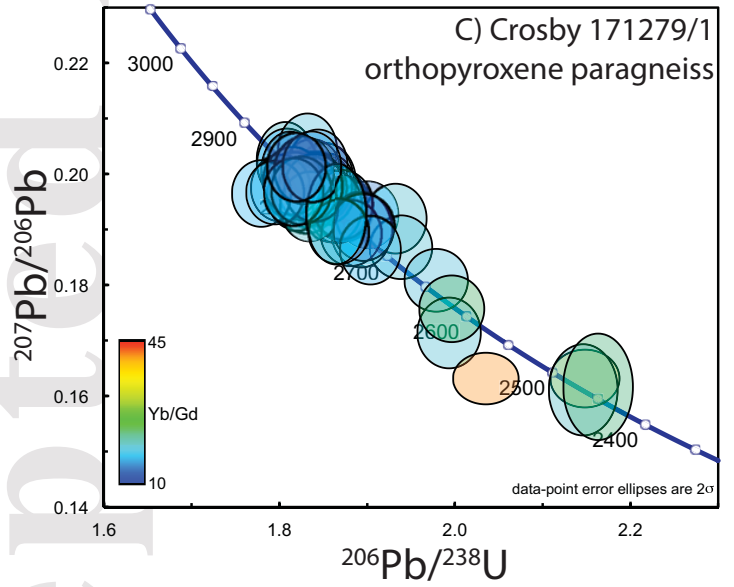

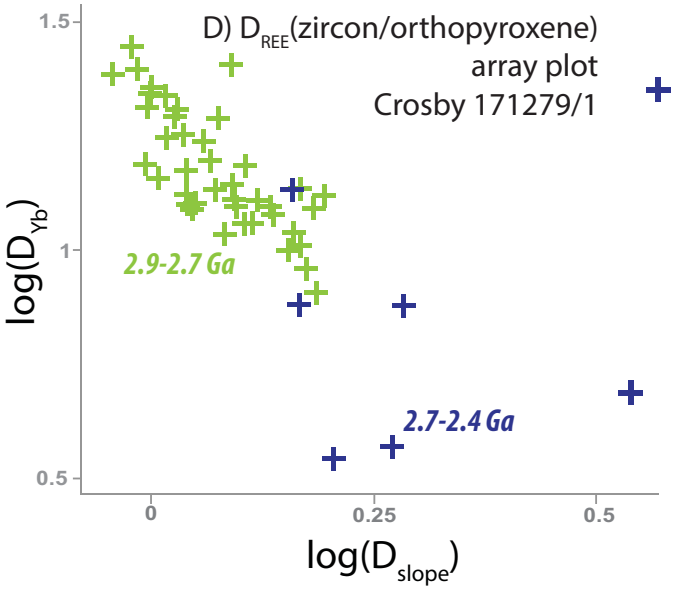

Figure 9